

Gap-dependent quasiparticle dynamics and coherent acoustic phonons in parent iron pnictide CaFe_2As_2 across the spin density wave phase transition

Sunil Kumar,¹ L. Harnagea,² S. Wurmehl,² B. Buchner,² and A. K. Sood^{1,*}

¹*Department of Physics and Center for Ultrafast Laser Applications, Indian Institute of Science, Bangalore 560012, India*

²*Leibniz-Institute for Solid State and materials Research, Dresden, D-01171 Dresden, Germany*

**asood@physics.iisc.ernet.in*

Using femtosecond time-resolved differential reflectivity measurements we investigate temperature and fluence-dependence of quasiparticle kinetics in iron pnictide CaFe_2As_2 single crystals exhibiting a spin density wave (SDW) and concurrent structural phase transition at $T_{\text{SDW}} \sim 165$ K. The fluence-dependence clearly shows that saturation effects dominate the behavior of the transient reflectivity signal at pump-fluences higher than $\sim 110 \mu\text{J}/\text{cm}^2$. Using pump-fluence well in the linear regime, we have analyzed the temperature-dependence of three-component carrier relaxation dynamics where the amplitudes and time-constants of the individual relaxation components show significant changes in the vicinity of T_{SDW} . In the SDW phase, using phonon-bottleneck model, temperature-dependence of the fastest electronic relaxation process yields the zero-temperature charge gap to be $2\Delta(0)/k_{\text{B}}T_{\text{SDW}} \sim 1.6 \pm 0.2$ whereas, in the normal state, an electron-phonon coupling constant of ~ 0.2 has been estimated from the linear temperature-dependence of the time-constant. Very low-frequency coherent oscillations with frequency in the gigahertz range are also observed which are attributed to coherent excitation of an acoustic phonon mode in the crystal. These measurements of acoustic phonons give the temperature-dependence of elastic modulus on either side of the phase transition temperature T_{SDW} .

PACS: 74.25.Gz, 78.47.J-, 75.30.Fv, 74.25.Dw

I. INTRODUCTION

Since the recent discovery of high temperature superconductivity in iron pnictides [1,2] a lot of interest has been generated, both theoretically and experimentally, to understand the magnitude, nature and symmetry of energy gaps in the spin density wave (SDW) and superconducting (SC) states of these compounds [3,4,5,6,7,8]. Parent compounds of the iron pnictide family show a spin-ordered phase below the SDW phase transition temperature (T_{SDW}) and superconductivity evolves either by electron or hole-doping at a lower temperature. Therefore, the parent compounds are being studied using various experimental methods to understand the role of spin fluctuations, spin-phonon and electron-phonon interactions. The picture on the nature and presence or absence of charge gaps opening at or below the magneto-structural transition in the parent compound so far remains inconclusive. On one side, the temperature-dependent resistivity indicates metallic behavior in the SDW phase [9,10]. Similarly, strong orbital-dependent reconstruction of the Fermi surface across the magneto-structural transition and metallic SDW state [11] or absence of charge gap [12,13] was derived from angle resolved photoemission spectroscopy (ARPES). On the other hand, in many infrared absorption studies [5,7,8] and a recent ARPES study [14], two charge gaps with $2\Delta_0/k_B T_{\text{SDW}}$ ranging between 3.5 to 11 have been reported. In the last two years, a few research groups [15,16,17] have studied the nature of charge gaps in the parent SDW iron pnictides: BaFe_2As_2 [15], SmFeAsO [16] and SrFe_2As_2 [17] in terms of charge quasiparticle dynamics using femtosecond time-resolved optical spectroscopy. The transient reflectivity measurements have shown a bi-exponential dynamics where a fast component could be described by quasiparticle recombination dynamics across a charge gap within the phonon-bottleneck model for gapped systems giving band gap value of $2\Delta_0/k_B T_{\text{SDW}} \sim 5$ [17] and 7.2 [16]. The slower relaxation process (time constant > 100 ps) was not analyzed in these studies [16,17].

There is an interesting difference, not yet understood, in the temperature dependence of resistivity of the parent and doped compounds from Ca-122 group; namely that a steep increase is seen in the resistivity at T_{SDW} [9,10], rather than a decrease as shown by Ba-122 and other types of pnictides [9]. Further, there is no femtosecond time-resolved study of parent and doped Ca-122 systems. Our present study addresses the temperature and fluence-

dependent quasiparticle dynamics using femtosecond pump-probe spectroscopy in parent CaFe_2As_2 single crystal with $T_{\text{SDW}} \sim 165$ K. Using a lower pump-fluence well in the linear regime, we have analyzed the temperature-dependence of the transient reflectivity whereas the saturation effects start affecting the signals at fluences higher than $\sim 110 \mu\text{J}/\text{cm}^2$. We clearly observe three distinct relaxation channels with decay times varying from subpicosecond to hundreds of picoseconds in the photoinduced differential reflectivity. Drastic changes in the amplitudes and decay-times of these electronic components occur at T_{SDW} which is an indication of charge gap in the spin density wave phase. Among these, only the fastest component that shows slowing down of the relaxation time and closing of a temperature-dependent band gap $\Delta(T)$ as one approaches T_{SDW} from below, was found to fit within the phonon bottleneck model described for the charge gapped systems [18,19,20]. We have derived the gap value $2\Delta_0/k_{\text{B}}T_{\text{SDW}} \sim 1.6 \pm 0.2$ from such an analysis. In the high temperature normal metallic phase of the sample, linear temperature-dependence of the relaxation time has been used to estimate the coupling strength of electrons with the optical phonons to be ~ 0.2 . Further, our experimental results, for the first time in a parent iron pnictide compound, clearly show the detection of very low-frequency coherent oscillations with frequency in the gigahertz (GHz) range superimposed on a slow exponentially decaying electronic-relaxation background. These are attributed to coherent excitation of an acoustic phonon mode launched by laser induced electronic and/or thermal stress at the sample surface. Analysis of the observed mode using strain pulse propagation model in the ultrafast ultrasonics [21] yields temperature dependence of the sound velocity and hence the elastic modulus across the SDW phase transition. Moreover, from the phonon-amplitude peaking at a temperature higher than T_{SDW} , we infer strong magneto-elastic coupling between spin-fluctuations in the normal paramagnetic phase and the lattice, a behavior similar to that observed in multiferroic manganites [22,23].

II. EXPERIMENTAL DETAILS

Single crystals of CaFe_2As_2 used in the present study were grown by high temperature solution growth technique using Sn flux and characterized as reported in Ref. [10]. Spin density wave phase transition along with a concurrent structural (S) transition from high

symmetry tetragonal phase to orthorhombic symmetry at low temperatures were established to occur at $T_{\text{SDW}} (T_s) \sim 165$ K. The crystals with c-axis perpendicular to the crystal surface were cleaved into platelet samples with thickness ~ 0.3 mm. Degenerate pump-probe experiments in a noncollinear geometry were carried out at 790 nm using 45 fs laser pulses at 1 kHz repetition rate taken from a regenerative amplifier. An aperture was placed about 30 cm before the sample in the path of unfocused pump and probe beams making the laser spot on the sample ~ 0.028 cm². The laser pulse energy was measured using a power meter (Spectra Physics, Model 407A) and the pump-fluence was varied from ~ 20 $\mu\text{J}/\text{cm}^2$ to ~ 175 $\mu\text{J}/\text{cm}^2$. To avoid the pump scattering in the pump-probe signal, we used pump and probe beam polarizations orthogonal to each other and the reflected probe light was detected with an analyzer crossed with the pump polarization. Continuous flow liquid-helium optical-cryostat was used to vary the sample temperature from 3.4 K to room temperature for temperature-dependent pump-probe measurements.

III. RESULTS

Experimental time-resolved differential reflectivity data at various sample temperatures using pump-fluence of ~ 85 $\mu\text{J}/\text{cm}^2$ are presented in Fig. 1. Overall, the transients can be decomposed into an electronic part (exponential decaying) and a coherent phononic part (damped oscillatory) using the following function convoluted with the Gaussian laser pulse,

$$\frac{\Delta R}{R} = (1 - e^{-t/\tau_R}) \left[\sum_k A_k e^{-t/\tau_k} + B e^{-t/\tau_p} \cos(2\pi\nu_p t + \phi) \right] \quad (1)$$

The term inside the small brackets takes care of the initial rise of the signals with a rise time of $\tau_R \sim 100$ fs, found to be independent of temperature and fluence. The first term inside the square brackets represent the electronic part with various amplitudes A_k and time-constants τ_k whereas the second term is the coherent part with amplitude B , dephasing time τ_p , frequency ν_p and initial phase ϕ . The data can be consistently fitted (solid lines in Fig. 1) with three electronic components ($k = 1,2,3$) and a single long wavelength oscillatory component attributed to coherent longitudinal acoustic phonon mode. We may mention that we could get good fits of the $\Delta R/R$ data using an expression

$[1 - \exp(-t/\tau_{R1})] * C_1 \exp(-t/\tau_1) + [1 - \exp(-t/\tau_{R2})] * C_2 \exp(-t/\tau_2)$ with just 5 fitting parameters ($C_{1,2}$, $\tau_{1,2}$ and τ_{R2}) instead of 6 ($A_{1,2,3}$ and $\tau_{1,2,3}$) as in Eq. (1). This way one obtains the values of slow rise time τ_{R2} behaving nearly the same as that for the slower relaxation time τ_2 in Eq. (1). However, we do not have a physical picture for such large values of the temperature dependent rise time τ_{R2} . Moreover, our later experiments on doped samples from the same Ca-122 series (Co doping $x = 0.056$) showed that the $\Delta R/R$ transients have an initial fast component followed by a neck at the intermediate time scales where it changes sign from negative to positive. Such a behavior can never be reproduced without taking a positive component ($+A_2, \tau_2$) at the intermediate time scales. Similar results were obtained for $x = 0.073$. Hence, for making a possible connection between the dynamics of undoped and doped compounds we have used Eq. (1) with fast rise time τ_R for both the undoped (present manuscript) and doped compound (unpublished). In Fig. 2 we plot the experimental data (open circles) and the fit (dark line) along with individual components (thin lines) for 3.4 K using Eq. (1). From such an analysis, we describe in detail the temperature and fluence-dependences of the carrier and coherent acoustic phonon dynamics in the following subsections.

The presentation of the results and related discussion is arranged as follows. First we discuss the temperature and fluence dependence of the carrier dynamics in section 3.1 and the coherent phonon results are discussed in section 3.2. We have used strain pulse propagation model in section 3.2 to derive temperature dependence of the sound velocity u_s and hence the elastic modulus Y from the observed phonon frequency ν_p and dephasing time τ_p . This, along with the temperature independent reflectivity value that is measured by focusing the femtosecond laser beam (low average power) and collecting all the reflected light for near-normal incidence angle allows us to estimate the refractive index n and the extinction coefficient κ (i.e. imaginary part of complex refractive index $n^* = n + j\kappa$) and hence the optical penetration depth $\zeta = \lambda/4\pi\kappa$ at laser wavelength λ . It is seen that ζ is almost 8 times larger at low temperatures than the value of ~ 42 nm at the room temperature, which renormalizes the amplitudes $A_{1,2,3}$ of the electronic relaxation components. Using the phonon bottleneck model [19], we have obtained a reduced charge gap value $2\Delta_0/k_B T_{SDW}$ in section 3.1 from the temperature dependence of A_1 below T_{SDW} .

3.1 Carrier dynamics

First we discuss temperature-dependent dynamics of the electronic part in the differential reflectivity signals. The results from the time-domain fitting (solid lines in Fig. 1) are presented in Fig. 3, clearly showing presence of one fast component (τ_1) with negative amplitude ($-A_1$), one slow component (τ_2) with positive amplitude (A_2) and a much slower component (τ_3) with negative amplitude ($-A_3$), all showing large variations around T_{SDW} . As T approaches T_{SDW} from below slowing down of the relaxation is clear from the increase in τ_1 and τ_3 (Figs. 3b and 3f) whereas decrease of τ_2 at T_{SDW} is evident from Fig. 3(d). Such sharp changes in the temperature-dependence of the three-component electronic relaxation amplitudes and time-constants at first instance may possibly give a clue to the opening of multiple gaps at T_{SDW} or an associated gap being anisotropic. Indeed, multiple charge gaps in the SDW phase of parent iron pnictides have been inferred from recent infrared spectroscopic [4,5,6,7,8] and ARPES [14] measurements. Theoretically, from the band structure calculations, it is known that the Fermi surface consists of two electron-like pockets at the M-point and three hole-like pockets at the Γ -point of the Brillouin zone [4,6]. Below T_{SDW} , opening of a gap in these pockets can give rise to the experimental observations.

Our results for the temperature-dependence of the fast component (A_1, τ_1) in the SDW state, shown in Figs. 3(a,b) are similar to earlier studies on parent BaFe_2As_2 [15], SmFeAsO [16] and SrFe_2As_2 [17], and can be fitted well within the phonon-bottleneck description of quasiparticle recombination across a temperature-dependent charge-gap $\Delta(T)$ as discussed in the following paragraphs. Moreover, we note another interesting aspect about the carrier dynamics from our results in Fig. 3. The amplitudes of all the three relaxation components are higher in the normal state ($T > T_{\text{SDW}}$) than in the SDW state ($T < T_{\text{SDW}}$). Though the drastic decrease in the amplitudes $A_{1,2}$ while approaching T_{SDW} from below is attributed to closing of charge gap (gaps) the larger magnitudes of the amplitudes in the normal state of CaFe_2As_2 is unusual with respect to the earlier studies on BaFe_2As_2 [15], SmFeAsO [16] and SrFe_2As_2 [17] where the amplitude corresponding to the order parameter was much smaller in the normal state. It appears that presence of spin fluctuations above T_{SDW} can be responsible for the large values of A_1 , A_2 and A_3 in the normal state showing maximum in A_2 and A_3 at ~ 220 K. As we will show in Section 3.2, these spin fluctuations can also be

responsible for the maximum in acoustic phonon amplitude B at a similar temperature suggesting existence of a characteristic temperature scale of ~ 220 K. We will come back to this discussion later in the section. We note that the pump-fluence of $\sim 85 \mu\text{J}/\text{cm}^2$ used for the present temperature-dependent dynamics is slightly higher than values used in previous pump-probe studies on parent iron pnictides [15,16,17,24] where amplified laser pulses with pulse repetition rate of 250 kHz or more were used and it was inferred that fluence of $\sim 20 \mu\text{J}/\text{cm}^2$ marks the end of the linear fluence regime. However, our experiments clearly show that for Ca-122 systems, the fluence saturation effects are seen only above $110 \mu\text{J}/\text{cm}^2$.

In the following we use the phonon bottleneck model derived by Kabanov et al., [19] for the temperature dependence of carrier dynamics in charge gapped systems considering that the photoexcited quasiparticle density at a fixed pump-fluence Φ is substantially less so that they make small perturbation to the distribution function of the normal state quasiparticle density. The amplitude (A) of photoinduced reflectivity signal is given by [19]

$$A \propto \frac{\Phi / (\Delta(T) + k_B T)}{1 + m \sqrt{k_B T / \Delta(T)} \exp[-\Delta(T) / k_B T]} \quad (2)$$

where m is a material-dependent constant. Assuming a BCS-like form $\Delta(T) = 2\Delta_0 \{1 - (T / T_{SDW})^2\}$ where $2\Delta_0$ is the zero-temperature value of the SDW gap, Eq. (2) describes an increase in the photoexcited quasiparticle density due to the decreasing gap value and corresponding enhanced phonon emission during the initial relaxation. As the gap closes at T_{SDW} , more low-energy phonons become available for reabsorption and the quasiparticle recombination mechanism becomes less and less efficient resulting in a quasi-divergence in the relaxation time given as [19]

$$\tau \propto \frac{\ln(g + \exp[-\Delta(T) / k_B T])}{\Delta(T)^2}, \quad (3)$$

where g is a fitting parameter. In order to use Eq. (2) to fit $A_1(T)$ values we should make sure that the amplitude values are normalized with respect to the absorbed energy per unit volume in the sample due to changes in optical penetration depth as a function of temperature at the probe wavelength. As mentioned before, from the analysis of the coherent acoustic phonon parameters using strain pulse propagation model (see section 3.2 for details) we realize that the optical penetration depth ζ is highly temperature dependent in CaFe_2As_2 (inset of Fig. 4c). The renormalized values of the amplitudes $A_{1,2,3}$ with respect to $\zeta(T)/\zeta(3.4\text{K})$ are plotted

in Fig. 4(a-c). Equation (2) is fitted to $A_1(T)$ in Fig. 4(a) for $T < T_{\text{SDW}}$ giving $2\Delta_0/k_B T_{\text{SDW}} = 1.6 \pm 0.2$. The solid line in Fig. 3(b) for $T < T_{\text{SDW}}$ is a fit to Eq. (3) with same value of $2\Delta_0/k_B T_{\text{SDW}}$. The value of $2\Delta_0/k_B T_{\text{SDW}}$ being less than the weak coupling limit of the BCS theory implies that there can be more than one gap opening at the SDW transition because in the phonon bottleneck model, the hot carrier relaxation is governed by the smallest energy gap in the system due to strong interband scattering [17]. The absence of a divergence in τ_1 as $T \rightarrow 0$ unlike in heavy Fermionic SDW compound UNiGa₅ [26] clearly indicates presence of ungapped Fermi surfaces at $T < T_{\text{SDW}}$ [17].

We may note that Eqs. (2) and (3) give the carrier dynamics for weak perturbation [19], i.e., the photoinduced carrier density n_s being smaller than the thermally generated carrier density n_T . In our case, we can estimate the photoinduced carrier density using $n_s = \Phi \alpha / h\nu_{\text{probe}}$ where Φ is the fluence and $\alpha = 1/\zeta$. From our present experimental results on the coherent acoustic phonons we have self-consistently derived a value of $\zeta \sim 320$ nm at the lowest temperature of 3.4 K. Taking $\Phi = 100 \mu\text{J}/\text{cm}^2$ and $\zeta \sim 320$ nm, unit cell volume = 170 \AA^3 (Ref. [27]), we obtain $n_s \sim 1.5 \times 10^{-3}$ /unit cell. Typical quasiparticle concentration in CaFe₂As₂ can be estimated [19] using the relation $n_0 = 2N(0)\Delta$ where $N(0)$ is the density of states at the Fermi energy. For CaFe₂As₂, $N(0) \sim 5$ /eV/unit cell (Ref. [28]) and $\Delta = 1.6k_B T_{\text{SDW}} \sim 20$ meV, we obtain $n_0 \sim 0.20$ /unit cell which is much larger than n_s . Furthermore, large changes in the temperature-dependent amplitudes and corresponding relaxation times of the electronic relaxation components measured at a fixed pump-fluence of $\sim 85 \mu\text{J}/\text{cm}^2$ (Fig. 3) clearly show that indeed n_T plays a major role in the carrier dynamics, thereby, justifying the use of the phonon-bottleneck model to analyze our results for A_1 , τ_1 while extracting the value of the band gap $2\Delta_0$.

The slow component (A_2, τ_2) in our studies (Figs. 3c and 3d) is unique and new as compared to the prior studies on parent iron pnictides [15,16,17] and cannot be described using the RT-model [18,19,20,25]. Here the amplitude A_2 has similar temperature-dependence as that of the fast one (A_1) but the decay time τ_2 shows a converging trend as $T \rightarrow T_{\text{SDW}}$ rather than the diverging behavior of τ_1 . Similar competing behavior of the fast and slow relaxation processes was seen in charge density wave systems [29,30,31] where the fast component with time constant $\tau \sim 0.5$ ps diverging at T_{CDW} was attributed to quasiparticle

recombination dynamics across the CDW gap whereas the slow relaxation with time constant $\tau \sim 7$ ps showed a large decrease while approaching T_{CDW} from below. This was initially attributed to collective excitations of the CDW state namely the phase mode [30]. However, in subsequent studies [29,31], τ_2 was assigned to the second stage of the CDW recovery. We believe that our observation of competing behavior of the fast (τ_1) and slow (τ_2) relaxation processes may be an indication of two sets of quasiparticles, either on different Fermi sheets around the Γ and/or M points or separately on two different Fermi sheets around these points in the Brillouin zone, competing for the density of states in the excited state. Alternately, this component could be simply ascribed to the lifetime of the optical phonons emitted during the charge gap quasiparticles recombination process where the sharp decrease in their lifetime at T_{SDW} means efficient energy release from photogenerated quasiparticles to these phonons. However, more theoretical understanding is yet to emerge.

The slower component (A_3, τ_3) can arise due to heat diffusion out of the photoexcited volume as suggested in Sr-122 and Sm-1111 iron pnictides [16,17] as well as from charged quasiparticle interaction with acoustic phonons and spin degrees of freedom [15].

So far we focused our discussion on the temperature-dependent carrier dynamics in the SDW state where the sharp changes in the amplitudes and corresponding time-constants of all three electronic relaxation components at T_{SDW} were attributed to opening of a charge gap. In the normal paramagnetic-metallic state ($T > T_{\text{SDW}}$), the temperature-dependent increase in the decay-time τ_1 (Fig. 3b) can be used to estimate the electron-phonon coupling constant λ using the relation [17] $\tau = 2\pi k_B T / 3\hbar \lambda \langle \hbar^2 \omega^2 \rangle$ where $\lambda \langle \hbar^2 \omega^2 \rangle$ is the second moment of the Eliashberg function. The linear fit (continuous line in Fig. 3b) gives $\lambda \langle \hbar^2 \omega^2 \rangle \sim 80$ meV². Taking $\langle \hbar^2 \omega^2 \rangle \sim 400$ meV² [17], we get electron-phonon coupling constant $\lambda \sim 0.2$, a case of weak electron-phonon coupling. This value of λ is similar to that obtained in SmFeAsO [16] and SrFe₂As₂ [17].

As we have pointed out earlier, the amplitudes of the three electronic-relaxation components are higher in magnitude in the normal state than in the SDW state ($A_{1,2,3}$ in Fig. 3) showing maximum in A_2 and A_3 at ~ 220 K. Figures 4(a-c) show that incorporating renormalization due to $\zeta(T)$, the characteristic temperature scale of ~ 220 K in CaFe₂As₂ becomes much clearer from the occurrence of a peak feature in the amplitudes (dashed lines

in Figs. 4(a-c) drawn as guide to the eyes). This particular feature of the carrier dynamics in CaFe_2As_2 is new as compared to earlier pump-probe studies on other types of parent iron pnictides [15,16,17]. The question to be asked is whether such a feature is related to stronger spin-phonon coupling just above T_{SDW} in the normal state of the iron pnictides or there exists a precursor pseudo state in the normal phase. In fact a peak in the coherent acoustic phonon amplitude B at a temperature higher than T_{SDW} (see Fig. 7a of section 3.2) can be attributed to strong magnetoelastic coupling. Interestingly, in a recent time-resolved experiment on BaFe_2As_2 , Kim et al., [32] showed that intense femtosecond laser pulses can induce transient SDW order parameter in the normal state, which again was explained in terms of strong spin-phonon coupling between spin fluctuations in the normal state and the optical phonons.

Time-resolved differential reflectivity data at various pump-fluences taken at four representative temperatures of 3.4 K, 90 K, 220 K and 300 K are presented in Fig. 5. The fluence-dependences of the electronic relaxation parameters obtained by fitting the data (fits are shown by solid lines in Fig. 5) using Eq. (1) are plotted in Fig. 6 in both the $T < T_{\text{SDW}}$ and $T > T_{\text{SDW}}$ regions. We note that the amplitude renormalization with respect to the temperature-dependent penetration depth as discussed above will not change the behavior of the fluence dependence of the amplitudes $A_{1,2,3}$ in Fig. 6. In the normal state ($T > T_{\text{SDW}}$), the amplitudes increase almost linearly with the increasing fluence as expected while the decay times remain fluence-independent. However, for $T < T_{\text{SDW}}$, saturation can be seen for all the three amplitudes (Figs. 6a, 6c and 6e). Also, the decay time τ_1 increases with the fluence (Fig. 6b). In the SDW state, linear increase in the amplitudes at low fluences and $\Phi^{1/2}$ dependence beyond a threshold indicate the gapped nature of the associated charge states as per the RT model [25]. However, the increasing behavior of τ_1 (Fig. 6b) is inconsistent with the RT model which rather predicts a linear increase in the quasiparticle relaxation rates, i.e., $1/\tau \propto \Phi$ [20,25]. In the prior studies on the parent compounds, the time constants associated with the carrier recombination in the SDW state were found to be fluence-independent [16,17] whereas, amplitude-saturation similar to ours was observed. The inconsistency with the RT model is not obvious from the present understanding of our temperature and fluence-dependent quasiparticle relaxation dynamics and needs to be explored further.

Finally, we draw attention to the possible implications of difference in the resistivity behavior of Ca-122 system as compared to other 122 systems as mentioned before in the

introduction. In the present study on parent Ca-122 system, we observe three electronic relaxation components which show dramatic changes at the SDW transition. Moreover, the relaxation component with relaxation time scale of ~ 5 ps is completely new and does not show a divergence at T_{SDW} but rather a competing nature with respect to the fast component (A_1, τ_1) across the SDW charge gap. On the other hand, for Ba-122 or Sr-122 parent compounds [15,17] only a single electronic relaxation component with amplitude following BCS-like temperature dependence was observed. Further, the value of the SDW gap measured in our experiments on Ca-122 is $2\Delta_0/k_B T_{\text{SDW}} \sim 1.5$ as compared to 3.5 to 4 in Ba-122 and Sr-122 systems [15,17]. This difference in the $2\Delta_0$ value has been attributed to the presence of multiple gaps in the Fermi surface across T_{SDW} . This may suggest that the nature of gaps in Ca-122 can be different from other 122 systems which may lead to different resistivity behavior. This has to be examined further.

3.2 Generation and detection of coherent acoustic phonons

Now we focus on the coherent part of the transient signals in Figs. 1 and 5. Temperature and fluence-dependences of amplitude B , frequency ν_p , dephasing time τ_p and initial phase ϕ of the coherent oscillations obtained from the time domain fitting (Eq. 1) are presented in Fig. 7(a-d) and Fig. 7(e-h), respectively, where dashed lines have been drawn as guide to the eyes. It is noteworthy to note that all the four parameters are highly temperature dependent across the SDW transition however they remain nearly fluence independent except the amplitude B which shows saturation with increasing fluence beyond $\sim 120 \mu\text{J}/\text{cm}^2$. In the vicinity of T_{SDW} , i.e., $T = 220$ K, the amplitude shows maximum coupling with the incident laser energy that tends to saturate at high fluences.

Generally, hot carriers generated by an ultrafast pump-pulse excitation can relax their energy via emission of phonons which cause oscillatory changes in the transient reflectivity signal. Coherent oscillations can also be induced by electronic and/or thermal stress at the photoexcited sample surface leading to strain pulse propagation into the sample with sound velocity u_s . The generation process of longitudinal acoustic phonons by strain-pulse propagation in the iron pnictide crystals is depicted in Fig. 8. The pump-pulse energy deposited at the surface of the crystal gives rise to transient electron and phonon-temperature

rise which then set up a transient stress via thermoelastic and/or electronic stress [21,33,34]. This stress is released by launching a strain wave in the form of coherent longitudinal acoustic (LA) wave propagating with sound velocity u_s into the crystal in the direction normal to the surface. The interference between the probe beams partially reflected from the interfaces defined by the crystal surface and the propagating strain pulse within the optical probe penetration depth is responsible for the detectable coherent oscillations in the reflectivity signal (for angle of incidence $\theta = 0$) [33],

$$\Delta R/R \propto k_{pr} \cos(2nk_{pr}u_s t + \phi), \quad (4)$$

k_{pr} being the probe wave-propagation vector, n the refractive index and ϕ the phonon phase. Therefore, the frequency of oscillations at a fixed probe angle of incidence θ is directly related to the sound velocity u_s and the probe wavelength λ_{pr} through the relation

$$\nu_p = 2nu_s \cos\theta / \lambda_{pr} \quad (5)$$

In the SDW phase the magnitude of the phonon amplitude B is nearly constant and much smaller possibly due to smaller thermal expansivity as compared to that in the normal state (Fig. 7a). Around T_{SDW} , B starts increasing and attains a peak feature at a temperature of ~ 220 K. This peak feature in the phonon-amplitude B at a temperature higher than T_{SDW} is similar to that was discussed before for the electronic relaxation components (Fig. 4). Such a feature may arise due to precursors of spin fluctuations in the normal paramagnetic phase [35,36] where large magneto-elastic coupling between spin fluctuations and lattice distortions can occur near the onset of SDW phase [37]. Similar precursor effect has been seen in the amplitudes of acoustic phonons in multiferroic manganites above the magnetic transition temperature and were attributed to the strong lattice coupling with the short range spin fluctuations [22,23]. The phonon-frequency ν_p is nearly constant in the deep SDW state but starts decreasing, as T_{SDW} is approached (Fig. 7b). The corresponding change in the phonon-phase ϕ by $\sim \pi/2$ (Fig. 7d) is a consequence of the structural transition which needs to be understood better.

The acoustic phonon-dephasing time τ_p also displays strong temperature dependence across T_{SDW} (Fig. 7c). In the strain pulse model, the dephasing of the oscillations can arise due to a combination of intrinsic phonon life time τ_{ph} and another contribution τ_α related to the probe absorption (α) within the optical penetration-depth ζ in the crystal [34]. The

phonon life-time corresponds to a time when the strain-pulse can propagate into the crystal within its characteristic length before complete energy transfer takes place from the coherent mode to a distribution of incoherent modes. For bulk samples, as is the case here, the strain pulse can propagate through the entire thickness of the sample and hence the observed phonon-dephasing τ_p in Fig. 7(c) should be limited by τ_α due to finite probe penetration depth. In fact, this provides an indirect way of measuring optical penetration-depth $\zeta = u_s \tau_p$ where u_s is the sound velocity and τ_p is identified as τ_α . We have to point out categorically that there is no report of the experimental value of the optical penetration depth at 790 nm at any temperature for Ca-122 systems in the literature. Sometimes the observed temperature dependences of the phonon dephasing time and phase can be attributed to the temperature dependent changes of the refractive index n and extinction coefficient κ as observed by Lim et al., [41] for LuMnO3 crystal where the probe wavelength is in proximity of the d-d optical transition peak that causes the refractive index and the extinction coefficient vary strongly with temperature. Based on the strain pulse propagation in combination with reflectivity value R , our experiments help to self-consistently estimate the temperature dependence of the refractive index n and the extinction coefficient κ (and hence optical penetration depth ζ) at 790 nm as described below.

We performed linear reflectivity measurements on our crystal by focusing the femtosecond laser beam (low average power) on the flat portion of the sample and collecting all the reflected light for near-normal incidence. The measured value is $R = 0.34$ which is constant as a function of temperature within an accuracy of $\pm 5\%$. We note that this value is very close to $R = 0.37$ as reported for Ba-122 iron pnictides at 790 nm [42]. As mentioned before, to be consistent with the strain pulse propagation model, the observed phonon dephasing at temperature T should correspond to the optical penetration depth ζ via the relation

$$\zeta(T) = u_s(T) \tau_p(T) \quad (6)$$

where the sound velocity $u_s(T)$ is related to $v_p(T)$ and the refractive index $n(T)$ via Eq.(5). Since $\zeta = \lambda_{pr} / 4\pi\kappa$, by incorporating Eq.(5) for normal incidence ($\theta = 0$) into Eq.(6), this relation simply leads to

$$\frac{n(T)}{\kappa(T)} = 2\pi v_p(T) \tau_p(T) \quad (7)$$

For normal incidence, the Fresnel's equation for reflectivity is given as

$$R(T) = \frac{(n-1)^2 + \kappa^2}{(n+1)^2 + \kappa^2} \quad (8)$$

Using constant value of $R = 0.34 \pm 0.2$ during 3.4 K to 300 K, we have estimated κ and n as a function of T from Eqs.(7) and (8) as shown in Figs. 9(a) and 9(b). The temperature dependent optical penetration depth ζ can be directly calculated from $\kappa(T)$ as shown in the inset of Fig. 4(c). It is noteworthy to see that the penetration depth changes from ~ 320 nm at 3.4 K to ~ 42 nm at 300 K leading to important consequences on the renormalization of the amplitudes ($A_{1,2,3}$) as shown in Figs. 4(a-c). Importantly, without any assumption, we have estimated the temperature dependence of n and κ from the experimental results for the frequency v_p and dephasing time τ_p of the acoustic phonon mode. We hope that our results will motivate detailed temperature dependent ellipsometry measurements of the optical constants of Ca-122 systems in future.

By knowing the temperature dependence of phonon frequency v_p and refractive index n , as discussed above, the temperature dependence of the sound velocity u_s can be calculated using Eq. (5) as shown in Fig. 9(c). The elastic modulus is obtained by using $Y = \rho \cdot u_s^2$, where ρ is the density of the crystal. The temperature-dependence of the density $\rho(T)$ of the crystal has been measured by x-ray diffraction which shows that unit cell volume of the CaFe_2As_2 lattice increases sharply at T_{SDW} [27]. We have used the mass of a unit cell $M_{\text{unit-cell}} \sim 96.98 \times 10^{-23}$ g and the temperature-dependent unit cell volume of CaFe_2As_2 from ref. [27] in estimating the density ρ (shown in the inset of Fig. 9d) and hence the elastic modulus Y of the crystal as presented in Fig. 9(d).

The temperature-dependence of the elastic modulus Y as shown in Fig. 9(d) is different than that measured using ultrasound measurements at MHz frequencies [38,39]. The latter shows that the elastic constants decrease as $T \rightarrow T_{\text{SDW}}$ from either side of T_{SDW} . This difference may arise from the difference in the coupling of sound waves of two frequencies with the slow relaxation processes in the system leading to dissipation and elastic dispersion [40]. In our case, the system relaxation time is as large as 500 ps ($\sim \tau_3$), which means that the observed acoustic waves in present experiments ($\omega \geq 1/\tau_3$) are in the zero-sound region (c_0).

On the other hand, the ordinary adiabatic (or first-sound) velocity ($c_1 < c_0$) is valid for $\omega \ll 1/\tau_3$. Therefore, the difference in the elastic properties measured using the present technique of ultrafast ultrasonics (GHz and above) and ultrasound spectroscopy (MHz and below) will depend on the difference between c_1 and c_0 and their temperature-dependences.

IV. CONCLUSIONS

Three-component quasiparticle relaxation is observed in CaFe_2As_2 iron pnictide single crystal on both sides of the spin density wave phase transition temperature. The amplitudes and time constants of all three relaxation components show large variations around T_{SDW} . Only the temperature-dependence of the fast relaxation process associated with quasiparticle recombination dynamics across a temperature-dependent charge gap could be described by the phonon bottleneck model. The temperature dependence of τ_2 below T_{SDW} , opposite to that of τ_1 , is similar to that observed in charge-density wave systems [29,30,31] and needs to be understood. Further, from the normal state temperature-dependence of the fastest relaxation time τ_1 , electron-phonon coupling constant is estimated to be ~ 0.2 . For the first time, our transient reflectivity data showed coherent longitudinal acoustic phonon oscillations over the entire temperature range that helped us in determining the crystal elastic behavior in both the normal as well as spin density wave phase. We hope that our experimental results will motivate further theoretical studies to understand the temperature-dependence of the second component (A_2, τ_2), sound velocity u_s and phonon phase factor ϕ as well as the maximum in the phonon amplitude B at temperatures higher than T_{SDW} .

ACKNOWLEDGEMENTS: AKS and SK acknowledge Department of Science and Technology, India for financial assistance. This work has been supported by the Deutsche Forschungsgemeinschaft through the Priority Programme SPP1458 (Grant No. BE1749/13), and through the Emmy Noether Programme WU595/3-1 (S.W.).

- [1] Y. Kamihara, T. Watanabe, M. Hirano, and H. Hosono, *J. Am. Chem. Soc.* **130**, 3296 (2008).
- [2] M. Rotter, M. Tegel, and D. Johrendt, *Phys. Rev. Lett.* **101**, 107006 (2008).
- [3] I. I. Mazin, D. J. Singh, M. D. Johannes, and M. H. Du, *Phys. Rev. Lett.* **101**, 057003 (2008).
- [4] L. Benfatto, M. Capone, S. Caprara, C. Castellani, and C. Di Castro, *Phys. Rev. B* **78**, 140502(R) (2008).
- [5] S. J. Moon, J. H. Shin, D. Parker, W. S. Choi, I. I. Mazin, Y. S. Lee, J. Y. Kim, N. H. Sung, B. K. Cho, S. H. Khim, J. S. Kim, K. H. Kim, and T. W. Noh, *Phys. Rev. B* **81**, 205114 (2010).
- [6] K. Nakayama, T. Sato, P. Richard, Y.-M. Xu, Y. Sekiba, S. Souma, G. F. Chen, J. L. Luo, N. L. Wang, H. Ding, and T. Takahashi, *Europhys. Lett.* **85**, 67002 (2009).
- [7] Z. G. Chen, T. Dong, R. H. Ruan, B. F. Hu, B. Cheng, W. Z. Hu, P. Zheng, Z. Fang, X. Dai, and N. L. Wang, *Phys. Rev. Lett.* **105**, 097003 (2010).
- [8] W. Z. Hu, J. Dong, G. Li, Z. Li, P. Zheng, G. F. Chen, J. L. Luo, and N. L. Wang, *Phys. Rev. Lett.* **101**, 257005 (2008).
- [9] G. Wu, H. Chen, T. Wu, Y. L. Xie, Y. J. Yan, R. H. Liu, X. F. Wang, J. J. Ying, and X. H. Chen, *J. Phys.: Condens. Matter* **20**, 422201 (2008).
- [10] L. Harnagea, S. Singh, G. Friemel, N. Leps, D. Bombor, M. Abdel-Hafiez, A. U. B. Wolter, C. Hess, R. Klingeler, G. Behr, S. Wurmehl, and B. Buchner, *Phys. Rev. B* **83**, 094523 (2011).
- [11] T. Shimojima, K. Ishizaka, Y. Ishida, N. Katayama, K. Ohgushi, T. Kiss, M. Okawa, T. Togashi, X.-Y. Wang, C.-T. Chen, S. Watanabe, R. Kadota, T. Oguchi, A. Chainani, and S. Shin, *Phys. Rev. Lett.* **104**, 057002 (2010).
- [12] C. Liu, G. D. Samolyuk, Y. Lee, N. Ni, T. Kondo, A. F. Santander-Syro, S. L. Budko, J. L. McChesney, E. Rotenberg, T. Valla, A.V. Fedorov, P. C. Canfield, B. N. Harmon, and A. Kaminski, *Phys. Rev. Lett.* **101**, 177005 (2008).
- [13] L. X. Yang, Y. Zhang, H.W. Ou, J. F. Zhao, D.W. Shen, B. Zhou, J. Wei, F. Chen, M. Xu, C. He, Y. Chen, Z. D. Wang, X. F. Wang, T. Wu, G. Wu, X. H. Chen, M. Arita, K. Shimada, M. Taniguchi, Z.Y. Lu, T. Xiang, and D. L. Feng, *Phys. Rev. Lett.* **102**, 107002 (2009).

- [14] P. Richard, K. Nakayama, T. Sato, M. Neupane, Y.-M. Xu, J. H. Bowen, G. F. Chen, J. L. Luo, N. L. Wang, X. Dai, Z. Fang, H. Ding, and T. Takahashi, *Phys. Rev. Lett.* **104**, 137001 (2010).
- [15] E. E. M. Chia, D. Talbayev, J.-X. Zhu, H. Q. Yuan, T. Park, J. D. Thompson, C. Panagopoulos, G. F. Chen, J. L. Luo, N. L. Wang, and A. J. Taylor, *Phys. Rev. Lett.* **104**, 027003 (2010).
- [16] T. Mertelj, P. Kusar, V. V. Kabanov, L. Stojchevska, N. D. Zhigadlo, S. Katrych, Z. Bukowski, J. Karpinski, S. Weyeneth, and D. Mihailovic, *Phys. Rev. B* **81**, 224504 (2010).
- [17] L. Stojchevska, P. Kusar, T. Mertelj, V. V. Kabanov, X. Lin, G. H. Cao, Z. A. Xu, and D. Mihailovic, *Phys. Rev. B* **82**, 012505 (2010).
- [18] A. Rothwarf and B. N. Taylor, *Phys. Rev. Lett.* **19**, 27 (1967).
- [19] V. V. Kabanov, J. Demsar, B. Podobnik, and D. Mihailovic, *Phys. Rev. B* **59**, 1497 (1999).
- [20] V. V. Kabanov, J. Demsar, and D. Mihailovic, *Phys. Rev. Lett.* **95**, 147002 (2005).
- [21] C. Thomsen, H. T. Grahn, H. J. Maris, and J. Tauc, *Phys. Rev. B* **34**, 4129 (1986).
- [22] K.-J. Jang, J. Lim, J. Ahn, J.-H. Kim, K.-J. Yee, J. S. Ahn, and S.-W. Cheong, *New J. Phys.* **12**, 023017 (2010)
- [23] K.-J. Jang, H.-G. Lee, .S. Lee, J. Ahn, J. S. Ahn, N. Hur, and S.-W. Cheong, *Appl. Phys. Lett.* **97**, 031914 (2010).
- [24] L. Stojchevska, P. Kusar, T. Mertelj, V. V. Kabanov, Y. Toda, X. Yao, and D. Mihailovic, *Phys. Rev. B* **84**, 180507(R) (2011).
- [25] J. Demsar, J. Sarrao, and A. J. Taylor, *J. Phys.: Condens. Matter* **18**, R281 (2006).
- [26] E. E. M. Chia, J.-X. Zhu, H. J. Lee, N. Hur, N. O. Moreno, E. D. Bauer, T. Durakiewicz, R. D. Averitt, J. L. Sarrao, and A. J. Taylor, *Phys. Rev. B* **74**, 140409(R) (2006).
- [27] S. Ran, S. L. Budko, D. K. Pratt, A. Kreyssig, M. G. Kim, M. J. Kramer, D. H. Ryan, W. N. Rowan-Weetaluktuk, Y. Furukawa, B. Roy, A. I. Goldman, and P. C. Canfield, *Phys. Rev. B* **83**, 144517 (2011).
- [28] E. Z. Kurmaev, J. A. McLeod, A. Buling, N. A. Skorikov, A. Neumann, M. A. Korotin, Y. A. Izyumov, N. Ni, and P. C. Canfield, *Phys. Rev. B* **80**, 054508 (2009).

- [29] A. Tomeljak, H. Schafer, D. Stadter, M. Beyer, K. Biljakovic, and J. Demsar, Phys. Rev. Lett. 102, 066404 (2009).
- [30] J. Demsar, K. Bijakovic, and D. Mihailovic, Phys. Rev. Lett. 83, 800 (1999).
- [31] A. Tomeljak, B. Kavcic, H. Schafer, V. V. Kabanov, D. Mihailovic, D. Staresinic, K. Biljakovic, J. Demsar, Physica B **404**, 548 (2009).
- [32] K. W. Kim, A. Pashkin, H. Schafer, M. Beyer, M. Porer, T. Wolf, C. Bernhard, J. Demsar, R. Huber, and A. Leitenstorfer, Nature Materials **11**, 497 (2012).
- [33] R. Liu, G. D. Sanders, C. J. Stanton, C. S. Kim, J. S. Yahng, Y. D. Jho, K. J. Yee, E. Oh, and D. S. Kim, Phys. Rev. B **72**, 195335 (2005).
- [34] S. Wu, P. Geiser, J. Jun, J. Karpinski, and R. Sobolewski, Phys. Rev. B **76**, 085210 (2007).
- [35] C. Fang, H. Yao, W.-F. Tsai, J. P. Hu, and S. A. Kivelson, Phys. Rev. B **77**, 224509 (2008).
- [36] V. Barzykin and L. P. Gorkov, Phys. Rev. B **79**, 134510 (2009).
- [37] H. Luetkens, H.-H. Klauss, M. Kraken, F. J. Litterst, T. Dellmann, R. Klingeler, C. Hess, R. Khasanov, A. Amato, C. Baines, M. Kosmala, O. J. Schumann, M. Braden, J. Hamann-Borrero, N. Leps, A. Kondrat, G. Behr, J. Werner and B. Büchner, Nature Materials **8**, 305 (2009).
- [38] M. A. McGuire, A. D. Christianson, A. S. Sefat, B. C. Sales, M. D. Lumsden, R. Jin, E. A. Payzant, D. Mandrus, Y. Luan, V. Keppens, V. Varadarajan, J. W. Brill, R. P. Hermann, M. T. Sougrati, F. Grandjean, and G. J. Long, Phys. Rev. B **78**, 094517 (2008).
- [39] R. M. Fernandes, L. H. VanBebber, S. Bhattacharya, P. Chandra, V. Keppens, D. Mandrus, M. A. McGuire, B. C. Sales, A. S. Sefat, and J. Schmalian, Phys. Rev. Lett. **105**, 157003 (2010).
- [40] Y. Ren, G. Lüpke, Y. Hu, Q. Li, C. S. Hong, N. H. Hur, and R. Merlin, Phys. Rev. B **74**, 012405 (2006).
- [41] D. Lim, R. D. Averitt, J. Demsar, A. J. Taylor, N. Hur, and S. W. Cheong, Appl. Phys. Lett. **83**, 4800 (2003).
- [42] L. Stojchevska, T. Mertelj, J.-H. Chu, I. R. Fisher, and D. Mihailovic, arXiv:1107.5934v1 (2011).

Figure captions

Fig. 1: Transient differential reflection spectra from CaFe_2As_2 as a function of sample temperature taken at a pump fluence of $\sim 85 \mu\text{J}/\text{cm}^2$. Solid lines are fits using Eq. (1).

Fig. 2: Experimental data (open circles) and fit (solid line) along with individual electronic components (thin lines) in Eq. (1) shown for 3.4 K presented for clarity of the data fitting procedure.

Fig. 3: Temperature-dependence of amplitudes A_k and decay times τ_k of three-component electronic relaxation obtained by fitting the experimental data in Fig. 1 with Eq. (1). The solid lines in (b) are theoretical fits as discussed in the text. The dotted vertical line marks the nominal SDW transition temperature.

Fig. 4: Amplitudes of the three electronic relaxation components ($A_{1,2,3}$) renormalized by the temperature dependent penetration depth $\zeta(T)/\zeta(3.4)$ at 790 nm as shown in the inset of (c). The solid line in (a) is theoretical fit using Eq. (2) and the dashed lines in (a-c) are drawn as guide to the eyes.

Fig. 5: Transient differential reflectivity as a function of the pump-fluence at four representative temperatures, two in the SDW and other two temperatures in the normal state of the sample. In each panel the data are plotted for five different values of the pump-fluence (20, 50, 85, 110, 175 $\mu\text{J}/\text{cm}^2$) increasing in the direction of the black arrow.

Fig. 6: Pump-fluence dependence of the amplitudes A_k and decay times τ_k of the three electronic relaxation components shown for temperatures from both the SDW and normal states of CaFe_2As_2 .

Fig. 7: Temperature and pump-fluence dependence of the amplitude B , damping time τ_p , frequency ν_p and initial phase ϕ of the coherent longitudinal acoustic phonon mode generated in CaFe_2As_2 . The solid lines are guide to the eyes.

Fig. 8: Schematic of the launching of a coherent strain wave in the direction normal to the surface in a propagating strain-pulse model. A strong pump-pulse creates a thermal strain at the surface ($z = 0$) which propagates into the medium with an average sound velocity u_s . Interference between the time-delayed (τ_d) probe pulses partially reflected from the interfaces defined by the front surface and the strain-pulse causes oscillations in the transient reflectivity signal.

Fig. 9: Temperature-dependent (a) extinction coefficient κ , (b) refractive index n , (c) longitudinal sound velocity u_s , and (d) elastic modulus Y derived from the temperature dependence of the acoustic phonon parameters as described in the text. The inset in (d) is the density ρ of the crystal taken from ref. [27] in combination with mass of unit cell $M_{\text{unit-cell}} \sim 96.98 \times 10^{-23}$ g that has been used to estimate the elastic modulus Y .

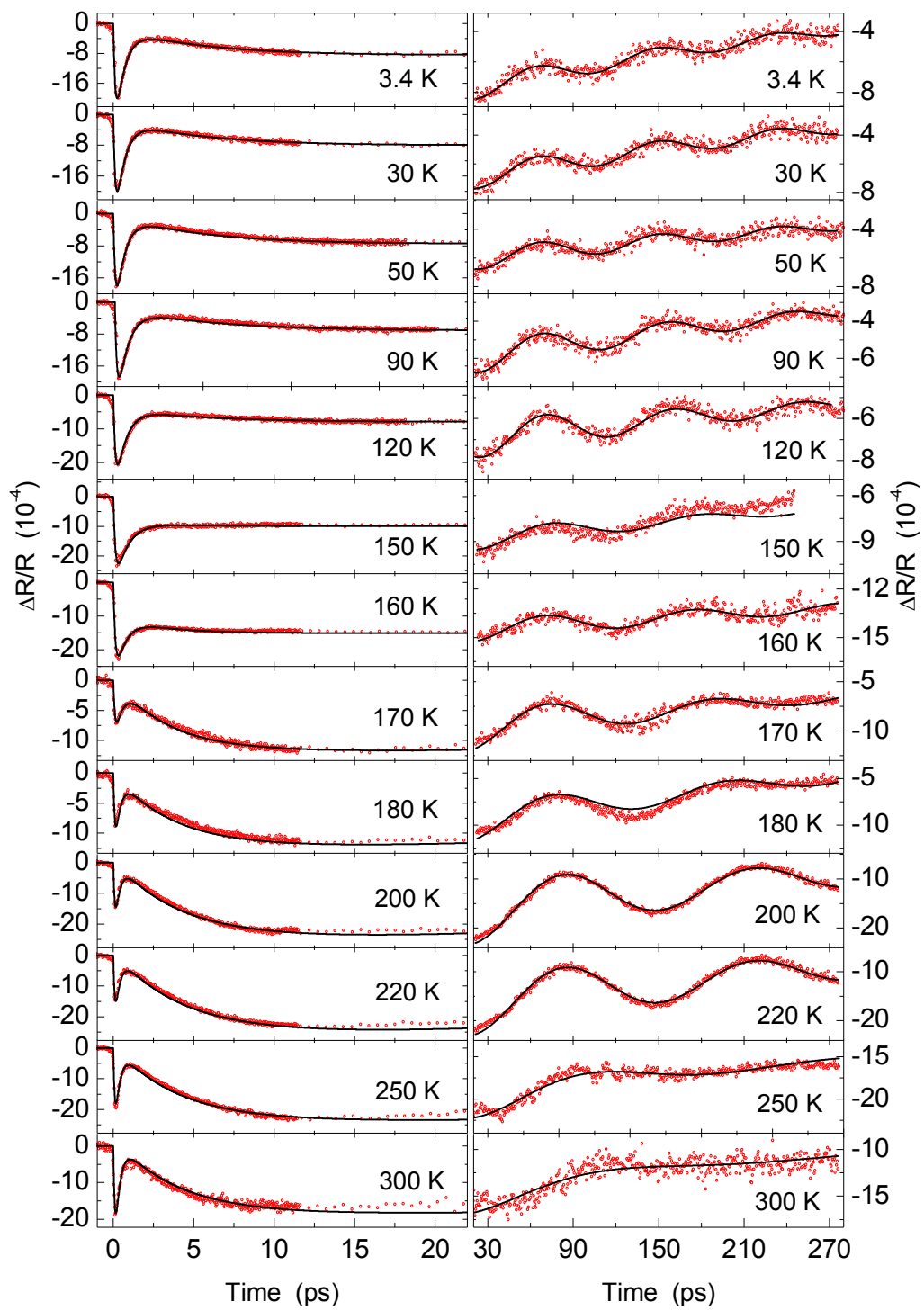


Figure 1

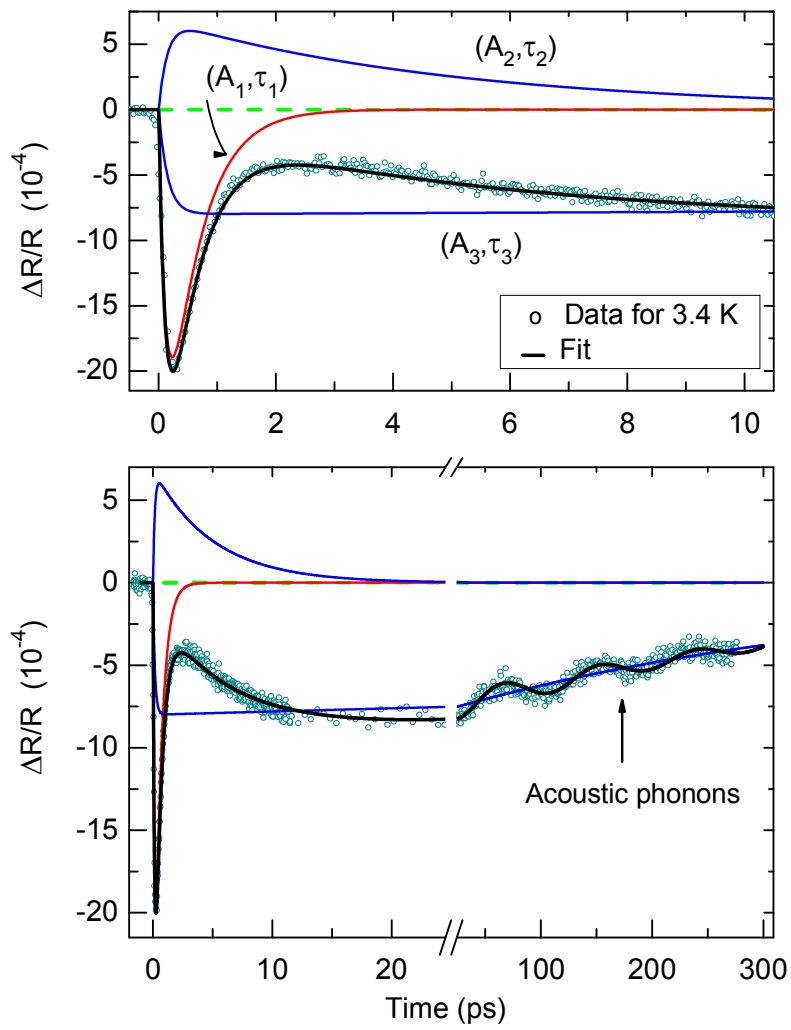


Figure 2

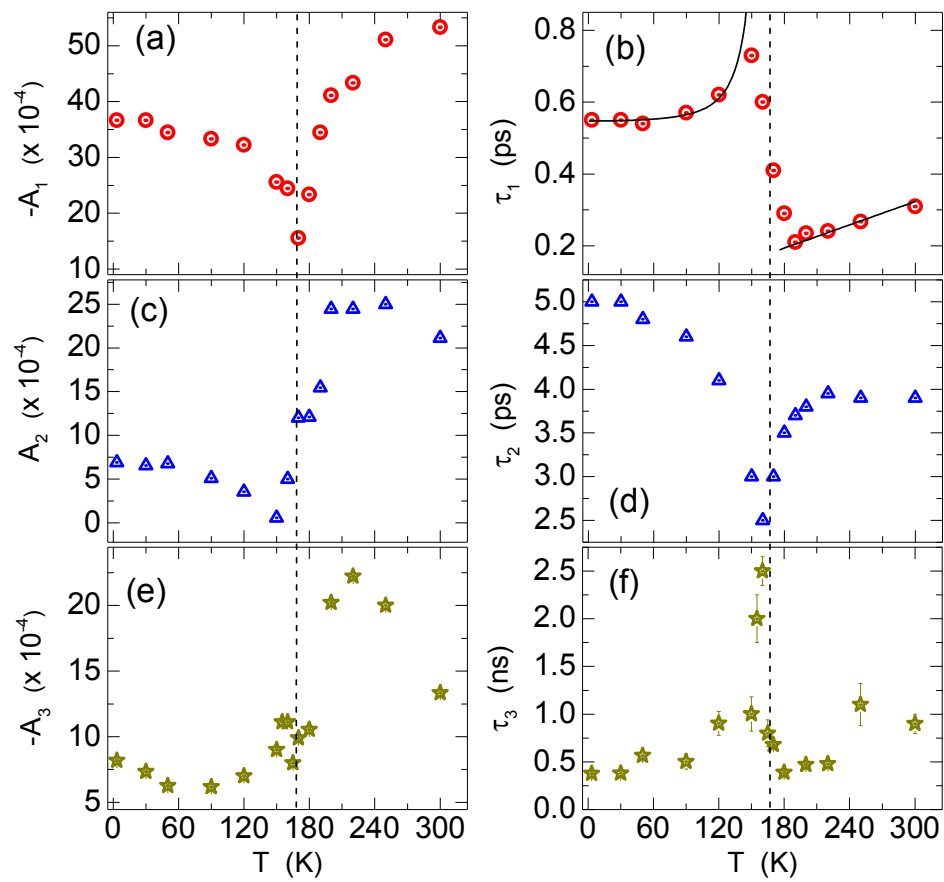


Figure 3

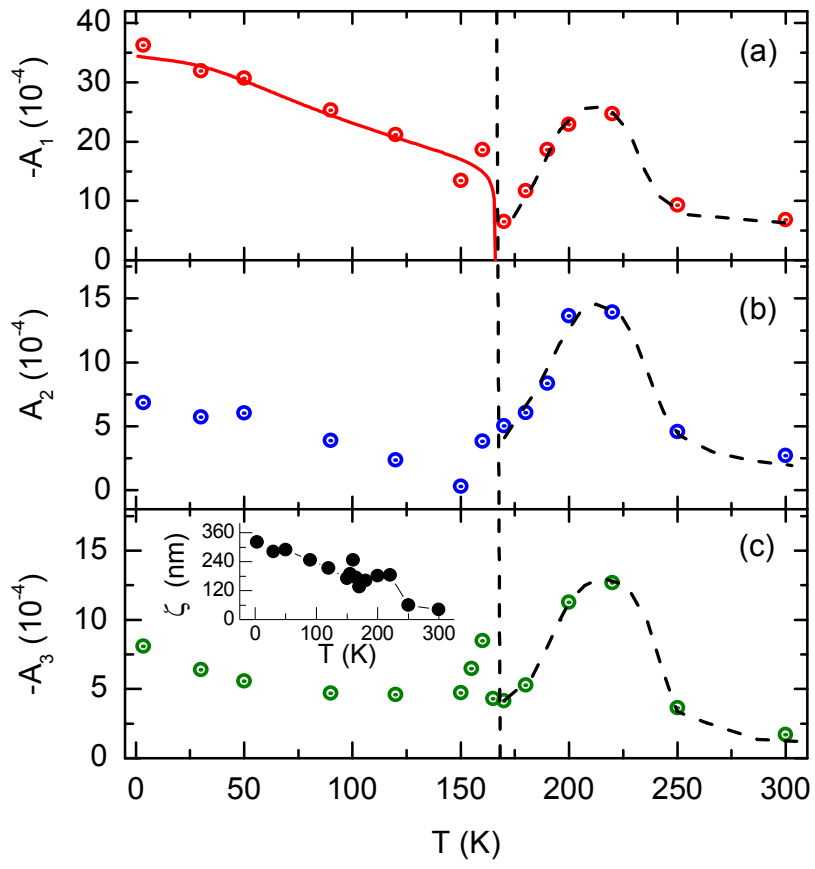


Figure 4

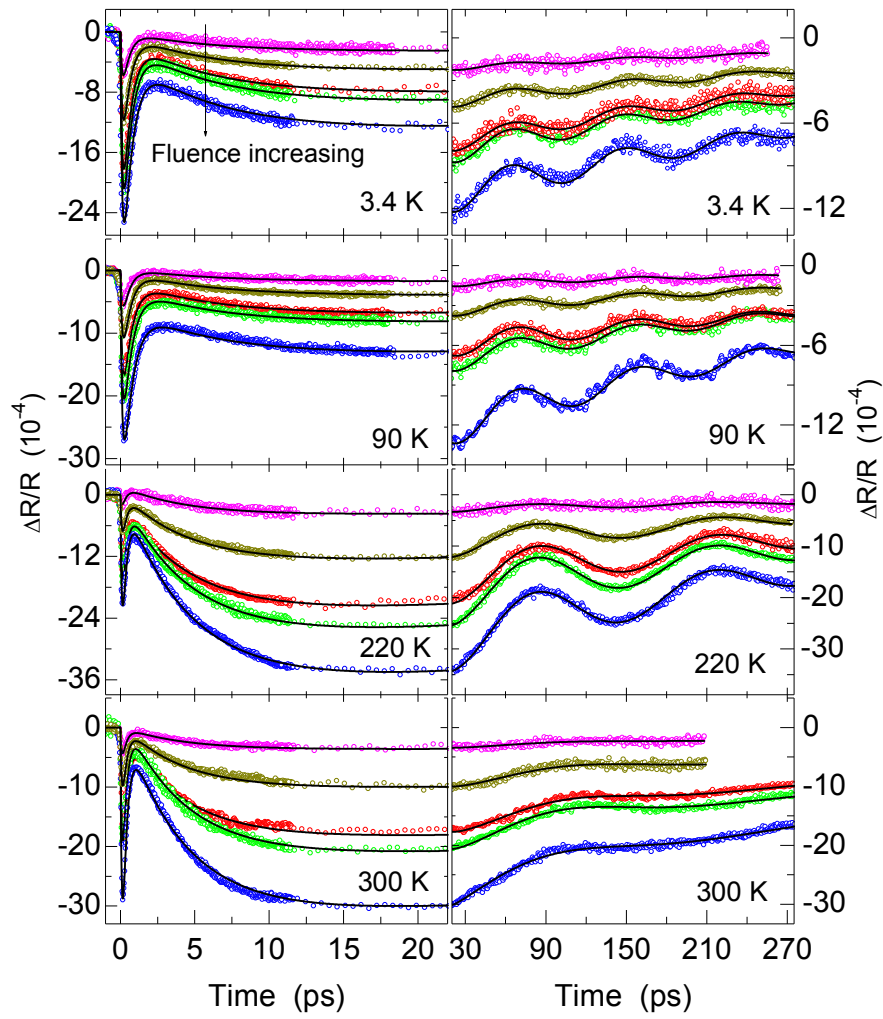


Figure 5

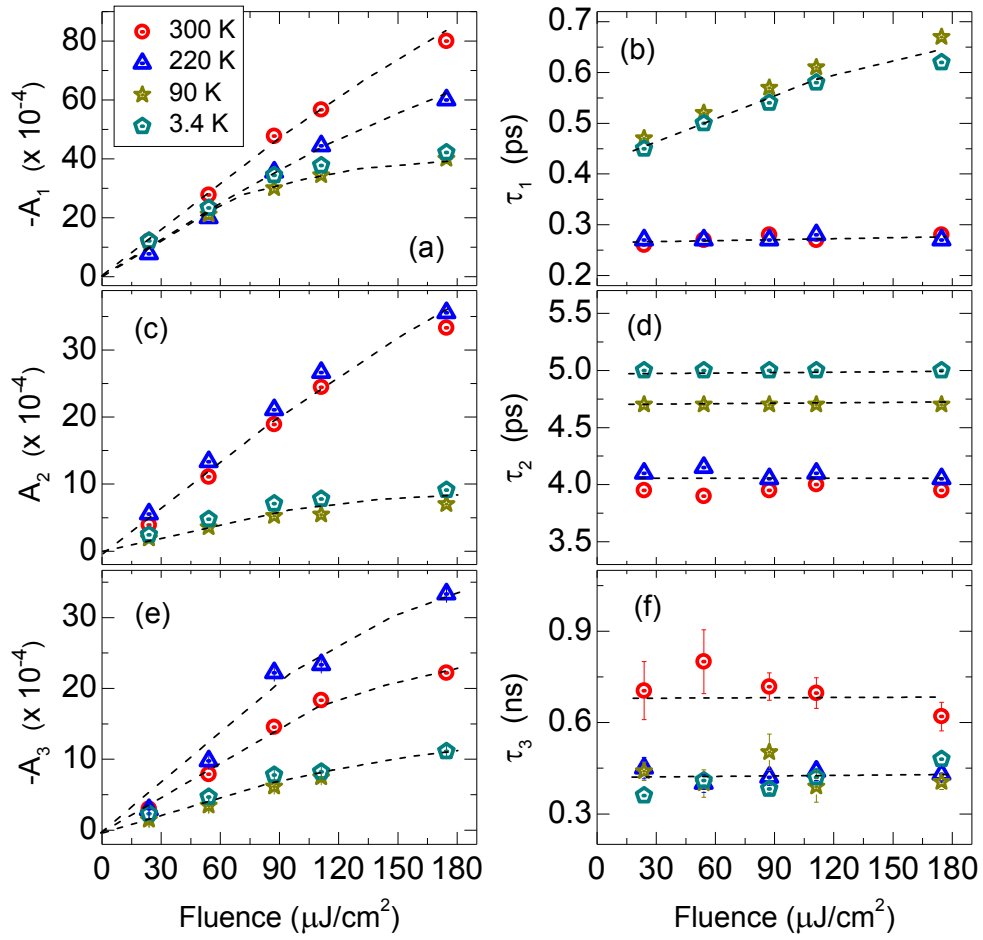


Figure 6

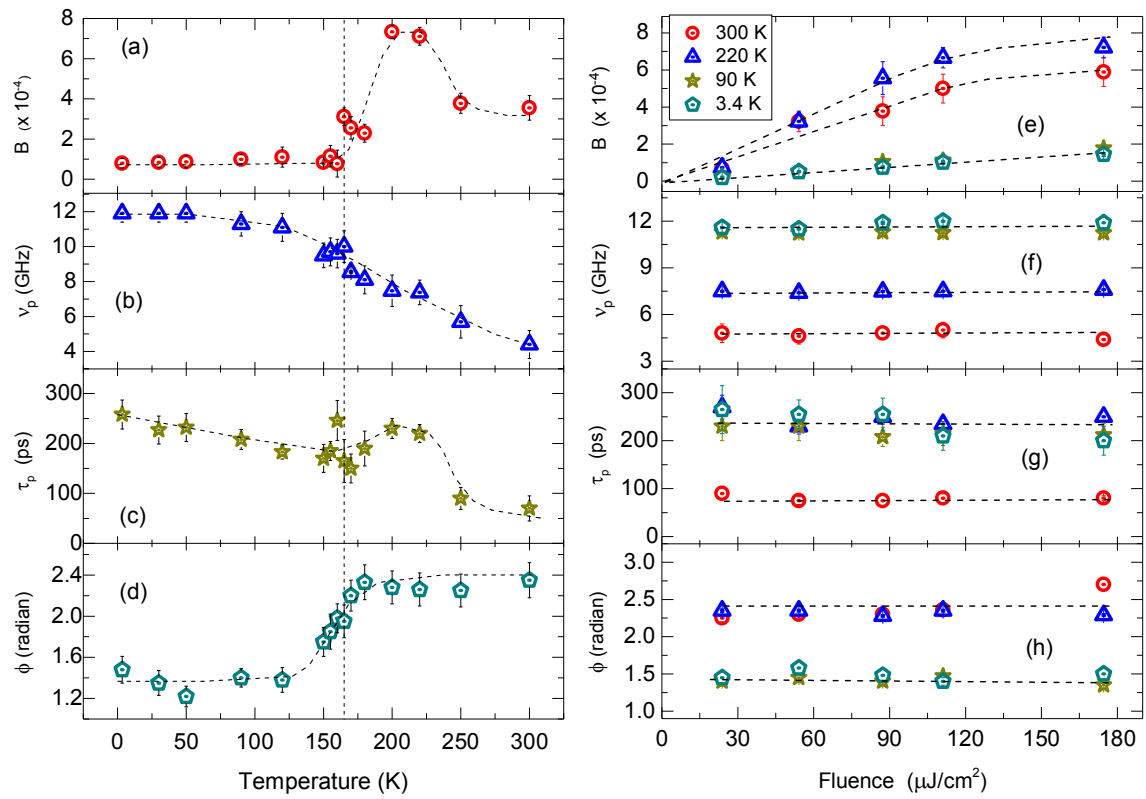


Figure 7

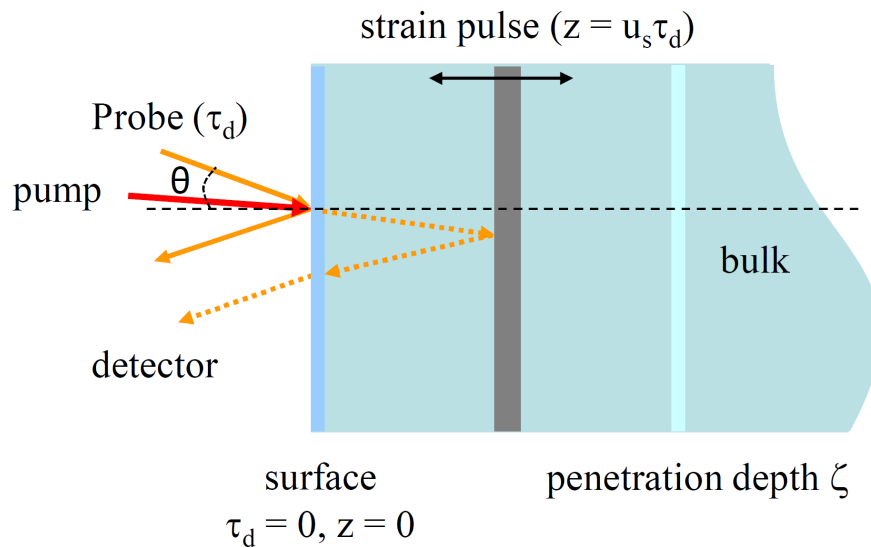


Figure 8

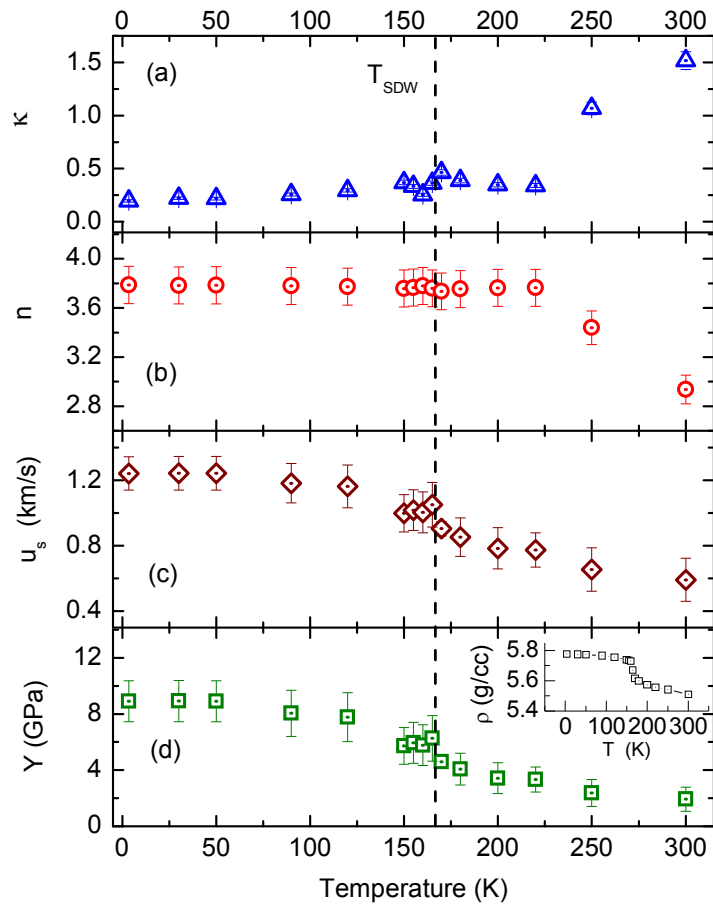


Figure 9